Proceedings of the
Annual Stability Conference
Structural Stability Research Council
St. Louis, Missouri, April 2-5, 2019

On the influence of load width on web compression buckling strength

Kadir Sener[1], Jacob Witte[2], Amit H. Varma[3]

Abstract
This paper presents an experimental and numerical study on web compression buckling strength of steel wide flange members subjected to concentric loads spread over lengths wider than the member depth. The AISC specification does not include loading width as a parameter for estimating web compression buckling strength, which can occur in steel connections. The strength equations for web compression buckling provided in the specification are limited to situations where the concentric compression load is applied over a very short length, for example, the flange thickness of the beam at beam-to-column (moment) connections. Limited analytical research has been conducted in the past to investigate the influence of load width on web compression buckling strength. Design equations proposed based on these prior (analytical) studies are limited to load widths less than or equal to section depth. This research aims to conduct experimental investigations and provide data that can be used to: (i) validate numerical models, and (ii) evaluate the effects of load width on the buckling strength under sustained loading conditions. Experimental investigations were conducted on wide flange steel members subjected to concentric compressive loading with load widths approximately equal to 2.5 times wider than the section depth. The experimental program also investigated the response of wide flange steel members to sustained loading, ranging from 80-to-90% of the direct strength, on web compression buckling strength. The experimental results were used to develop and benchmark numerical (3D finite element) models. These models accounted for the effects of geometric imperfections, residual stresses and material inelasticity. The benchmarked models can be used to conduct additional numerical parametric studies.

1. Introduction

AISC Specification Section J10 discusses the limit states associated with flanges and webs of wide flange members subjected to concentrated forces. Of the three compressive force buckling related limit states, only web compression buckling in Section J10.5 does not account for load width when determining the available strength of the limit state. The web compression buckling limit state was

[1] Research Engineer in Civil Engineering, Purdue University, <ksener@purdue.edu>
[2] Graduate Research Assistant in Civil Engineering, Purdue University, <witte3@purdue.edu>
[3] Karl H. Kettlelhut Professor in Civil Engineering, Purdue University, <ahvarma@purdue.edu>

primarily developed for beam-to-column moment connections where the beam flanges could apply a concentrated compression force onto the web of the column. The beam flanges have relatively small thickness, thus producing a negligible load width to be considered. However, there are other common instances where concentrated forces are applied to the webs of wide flange sections over a significant load width.

It can be inferred that if a large concentrated force is applied over a length larger than the depth of the specimen, the available strength could be greater than that of the same concentrated force applied over a small load width. However, the current AISC equation for web compression buckling does not account for load width. This paper examines the validity of that inference, the ability to accurately predict the buckling strength with numerical modeling and explore the effects of sustained loading onto the onset of web compression buckling. Most of the knowledge on the creep effects (or lack thereof) in steel has been obtained through uniaxial tension tests, such as those conducted by Cheng et al (2001). The tests conducted show that steel creep deformations are negligible at room temperature. Therefore, this paper explores if these results also hold true in the case of web compression buckling, particularly when the sustained load is in the range of 80-90% of the strength.

2. Objective

The investigation of the influence of load width on web compression buckling is a relatively new area of research. One of the most recent papers on this topic was authored by Menkulasi et al. (2016). Their paper explored the effects of load width on the web compression buckling limit state but was limited to widths less than the section depth and did not feature any experimental verification of their findings. This paper will explore web compression buckling behavior for load widths greater than the section depth using both numerical and physical experimental results.

3. Experimental Testing

A series of tests were conducted to evaluate the influence of load width on the limit state of web compression buckling. Two tests were conducted monotonically, i.e., the applied loading was increased gradually up to web compression buckling. And, two additional tests were conducted where the applied loading was first increased gradually to about 80-90% of the peak force from the monotonic tests, maintained for several hours to evaluate the effects of sustained loading, and then increased gradually up to web buckling. The specimens were selected to be 42-inch long segments of ASTM A992 Gr50 W18x40 beams. Certified mill test report (CMTR) of the W18x40 sections indicated the yield and tensile strengths were 57 ksi and 75.5 ksi, respectively.

3.1 Specific Objectives

The primary goal of the experimental testing was to obtain behavioral data and results under loading and boundary conditions that can be modeled and replicated in a numerical model. The details of the numerical model can be benchmarked using experimental results and the actual behavior of the specimens, thus improving the level of confidence in the models. The benchmarked models can then be used to conduct analytical parametric studies. Another goal of the experiments was to evaluate the influence, if any, of sustained loads (in the range of 80-90% of the buckling strength) on the behavior and web compression buckling of the specimens.

3.2 Test Setup

Figure 1 illustrates a schematic drawing of the test setup described in this section. The specimen, shaded in green, is secured to the platform with 20 fully tensioned 3/4 in. A325 high strength bolts, 10 on each side of the flange. This bolt pattern ensures that the entire length of the bottom flange is fully restrained from rotating and pulling away from the platform. The large spreader beam is similarly bolted to the top flange of the specimen ensuring the two of them to move as one assembly. The load frame, shaded in blue carries the cylindrical actuator, and provides a support for the lateral braces (see Figure 1) to react against. These braces prevent any out of plane movement in the spreader beam, thus restricting the top flange of the specimen from rotation as the load is applied. Load cells were placed in between the load frame and the lateral braces to measure the bracing force (if any). The load frame was built of heavy wide flange sections with large axial and flexural stiffnesses providing quasi-rigid reactions. Both the platform and the load frame are secured to the lab floor using 1-1/4 in. and 1-5/8 in. diameter post tensioning bars respectively.

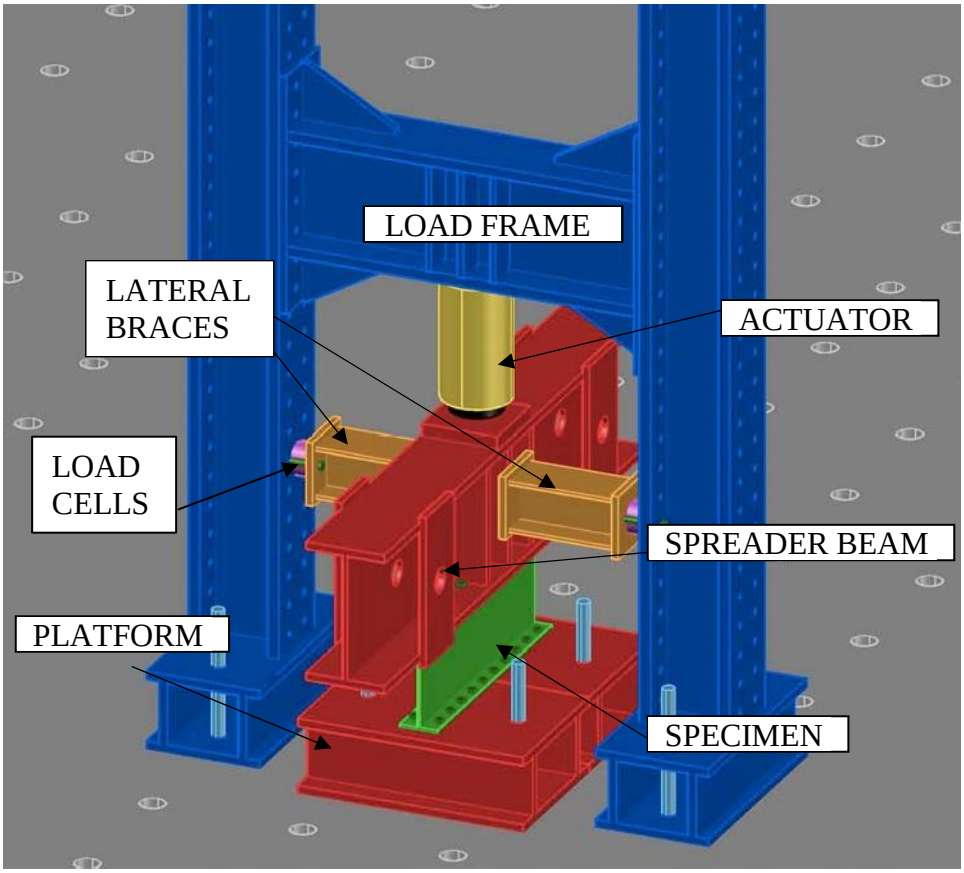

Figure 1: Test Setup Schematic

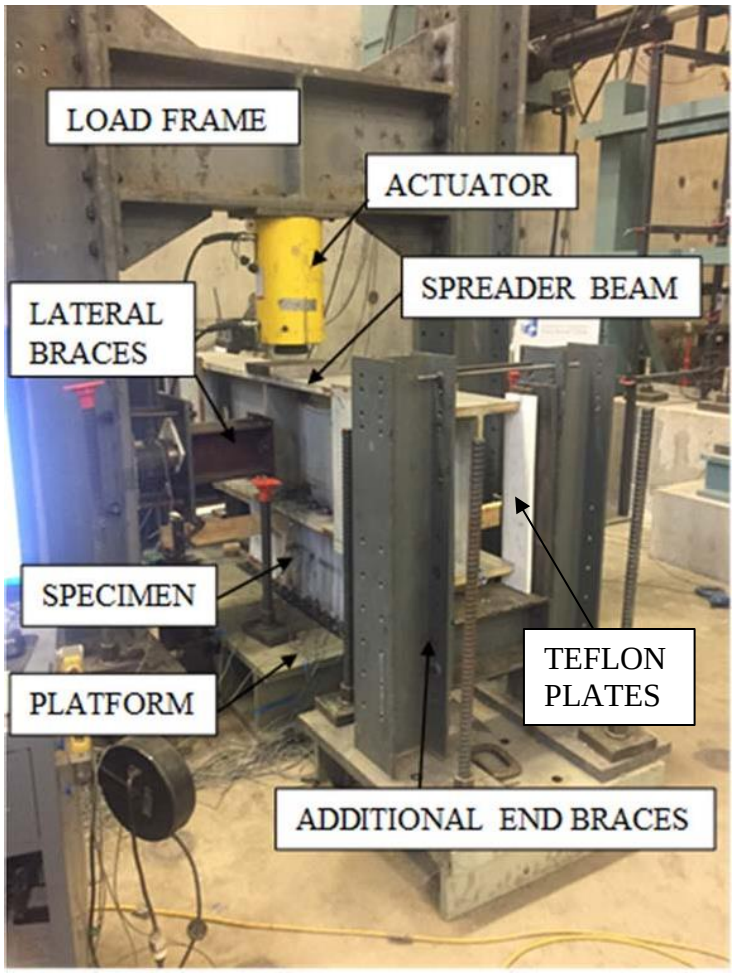

Figure 2: Completed Test Setup

Figure 2 shows a photograph of the test setup on the laboratory strong floor used to conduct the experiments. After the initial commissioning of the setup, the spreader beam was restrained against out-of-plane twisting. Additional end braces were installed along with the lateral braces in the middle, thus restricting the spreader (loading) beam from twisting. White Teflon plates were added at all contact surfaces to minimize any friction between the spreader beam and the braces. These loading, boundary, and bracing conditions were modeled and replicated by the numerical models.

3.3 Instrumentation

The load-deformation behavior and the structural response of the specimens was observed and measured using several instruments and sensors. Additional sensors were also used to monitor the behavior of the loading test setup. Strain data was recorded using strain gauges applied to both faces of the specimen web along the section depth midline. Displacements were measured using displacement transducers (DTs) with 1 in. stroke placed at various locations.

Figure 3 is a graphical representation of the instrumentation used in Tests 1 and 2. A total of 8 strain gauges (S#) were applied to the web. On each face, one strain gauge (S3-S4) was applied vertically at the midpoint of the specimen with two more vertical gauges applied 6 in. away from the midpoint (S1-S2, S7-S8), but still on the midline of the section depth. A fourth gauge was applied horizontally to measure transverse strains close to the web midpoint (S5-S6). This gauge

layout was mirrored on the other face of the web. To measure the vertical deflection (DT#) of the top flange, two displacement transducers were placed at the midpoint along the length each side (DT1- DT6). This created redundant data that provided a high level of confidence in the test setup and provided the ability to confirm the absence of any rotation in the top flange. On one side only, two additional DTs were placed 12 inches in each direction away from the midpoint to capture any variance in the top flange vertical deflection along the length of the specimen (DT2-DT5). There is also one transducer placed horizontally at the midpoint of the web to capture the out of plane displacement as buckling occurs (DT7). Inclinometers (CM#) were also installed on both ends of the spreader beam, to track any rotation of the top flange (CM1-CM2). The data from the inclinometers was used in tandem with the redundant DTs at the midpoint of the vertical flange to confirm adequate performance of the test setup.

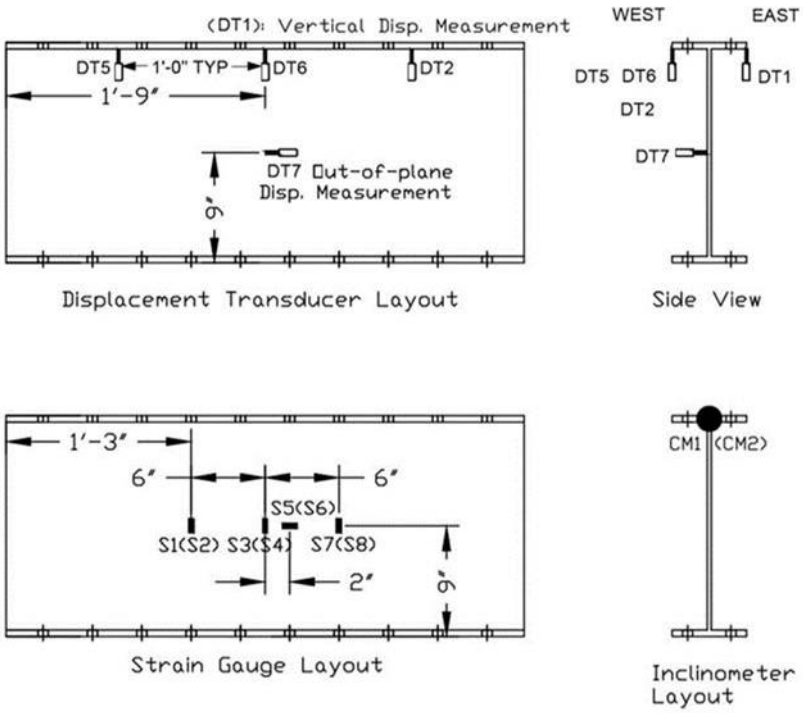

Figure 3: Instrumentation Layout used in Tests 1 and 2

After examining the results from the first 2 tests, the need for additional sensors became apparent. Similar to the approach used to measure vertical flange displacement at various points along the length of the specimen, the web out of plane displacement also needed to be measured along the length. Additionally, due to the high compressive forces involved with the test, the platform supporting the specimen (see Figure 1 and Figure 2) experienced minor displacements that went unnoticed during the first two tests. This resulted in downward motion of the top flange not only due to axial deformations in the web, but also due to deformations of the platform. To account for this, DTs were placed along the bottom flange directly underneath where the top flange displacement was measured. This enabled calculation of the relative (net) displacement of the flanges, which is the true deformation in the web.

Figure 4 shows the modified instrumentation layout developed to address these needs. Instrumentation layout at the three locations that previously had vertical DTs at the top flange were

updated to also have a group of three DTs measuring: vertical displacement in the top flange, out of plane displacement in the web, and vertical displacement at the bottom flange. This new layout provided both relative flange displacement and web out-of-plane displacement data at different sections along the length of the specimen. Four more strain gauges were added further away from the loaded mid-region of the specimen to evaluate the difference between strain data toward the ends of the specimen versus those in the middle. These additional data from the new sensor layout created a more complete picture of the specimen response.

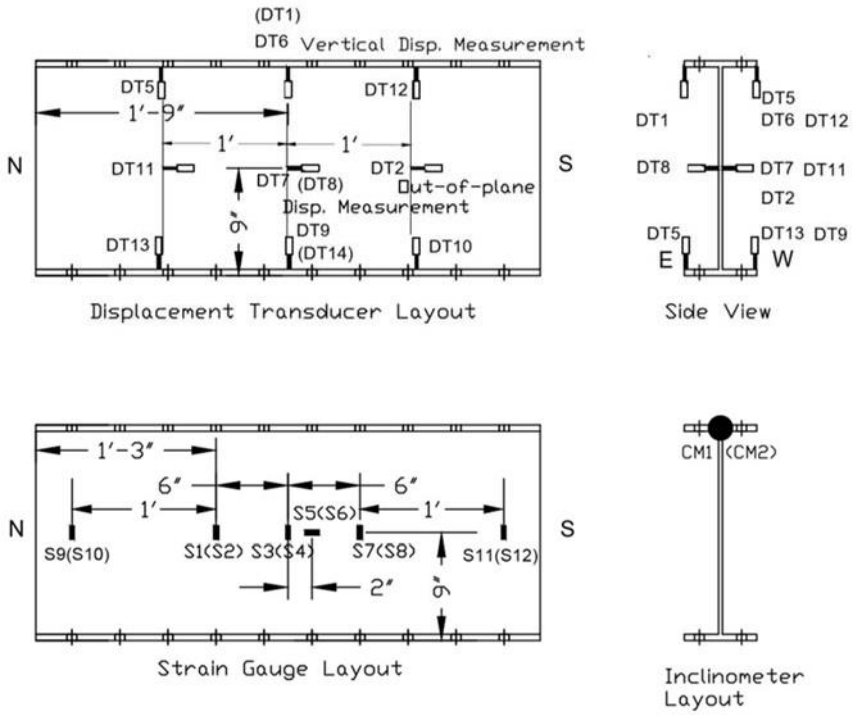

Figure 4: Modified Instrumentation Layout used in Tests 3 and 4

3.3 Loading Protocol

As mentioned earlier, two tests were conducted monotonically, and two tests included a sustained load portion. The monotonic loading simply consisted of quasi-statically increasing the load applied to the specimen until buckling occurred. The quasi-statically loaded tests were conducted first, so that the buckling strength of the specimens could be obtained. These tests provided valuable data in terms of fundamental load-displacement-strain response and also about experimental behavior while subjected to the specific loading condition. The first two tests also enabled establishing a sustained load protocol to conduct the latter two tests.

Tests 3 and 4 were initially loaded monotonically until the target sustained load level was reached, which was followed by implementing a sustained load protocol. These specimens were loaded to approximately 80-90% of their buckling strength, then the load was sustained for periods of 2.5 hours and 4 hours in Tests 3 and 4 respectively. The monotonic buckling strength of specimens during the Tests 3 and 4 was estimated without utilizing a design equation. The target sustained load level was obtained based on the consistent experimental behavior observed for the monotonically loaded specimens, by examining patterns in the strain data as the specimen approached buckling. This process is further discussed later in this paper. After the load was

sustained for the prescribed length of time, the load applied to the specimen was increased gradually until buckling occurred.

4. Numerical Modeling

Numerical models of the tested specimens were developed in the finite element software Abaqus using the available 3D solid element library. The reduced integration solid element (C3D8R) was used throughout the models with very fine mesh density, by having four elements through the thickness of the web.

The analyses were performed using the Abaqus/Implicit solution method. Sequential analyses were conducted by first performing an eigenvalue frequency analysis using the buckling analysis technique in Abaqus. Initial imperfections for the latter structural analysis stage was determined during the eigenvalue analysis. Boundary conditions for both the analysis replicated the test case by restraining all the rotations and translations on both flanges, except releasing the top flange movement in the vertical direction. A notional vertical load was applied on the top flange to initiate the analysis.

Structural analysis was conducted with different amplitude levels of initial imperfections by varying the peak imperfection from 0.1-times the web thickness ($0.1t_w$) to 0.3-times the web thickness ($0.3t_w$). This corresponds to a web imperfection amplitude of 0.0315 inches to 0.0945 inches, respectively. Only the first mode shape was considered for initial geometric imperfection, as this mode shape correlated with the buckling mode observed during the physical test of the specimens. Preliminary finite element analysis conducted to investigate the influence of residual stresses on web compression buckling indicated negligible effects. This was due to residual stresses mainly generating influence in the longitudinal direction, but having minimal influence in the direction of vertical stress components.

Structural analysis was performed using the modified-Riks analysis method in Abaqus to capture the response in both pre and post-buckling stages. Identical boundary/load conditions were prescribed in the static Riks analysis as the eigenvalue analysis. The steel material was modeled using multiaxial plasticity theory with von-Mises yield surface, associated flow rule, and isotropic hardening. Steel Young's modulus and Poisson's ratio was set equal to 29000 kips per square inch (ksi) and 0.3, respectively. The steel-stress strain response was obtained using the measured yield and tensile strength reported in the CMTR's of the steel specimens. The reported yield and tensile strength properties were used to generate a realistic stress vs. plastic strain relationship for input. This relationship was obtained by a spreadsheet that was developed by the authors by characterizing stress-strain behavior of similar steel materials from an experimental database.

Numerically obtained vertical load vs. vertical or out-of-plane displacement responses corresponding to each imperfection level were compared with experimental results.

5. Experimental Results and Comparisons

5.1 Monotonic Experimental Responses

The results observed in the experimental tests were compared with those generated by the numerical model. The ultimate buckling load of the four specimens was determined. For the specimens that were subject to sustained loading, the percentage of the ultimate strength that was sustained was calculated. These results are summarized in Table 1, and the nominal available strength in web compression buckling calculated using the existing AISC equation J10-8 is provided in the footnote. The mean strength from the four tests is 341 kips. The standard deviation is 14 kips (or 4% of the mean value).

Table 1: Experimental and Numerical Buckling Strengths

Experimental			Numerical	
Test	Observed Strength (kips)	Percent of Strength Sustained	Initial Imperfection	Predicted Strength[1] (kips)
1	341.3	-	$0.1t_w$	365.5
2	359.3	-	$0.2t_w$	346.6
3	342.8	91	$0.3t_w$	327.6
4	320.1	83		

1. AISC predicted strength: 58 kips

Figure 5 and Figure 6 show the comparison between the monotonic experimental results and the finite element analysis. The solid horizontal line marked by point 1 shows the nominal available strength in web compression buckling (R_n) calculated using the existing AISC equation J10-8, shown below as Eq. 1:

$$R_n = \left(\frac{24t_w^3\sqrt{EF_{yw}}}{h}\right)Q_f \tag{1}$$

The parameters in the above equation are defined as follows: t_w is the thickness of the web, E is the elastic modulus of steel, F_{yw} is the yield strength of the web material, h is the clear distance between the flanges less the corner fillet (also defined as T in Part 1 of the AISC Manual), and Q_f is a shape factor set to 1.0 for rolled shapes. According to this equation, the nominal available strength of the specimens tested (W18x40 section of A992 Gr50 steel) in web compression buckling would only be 58 kips, using the measured yield strength. On the other hand, the experimental results demonstrate specimen strengths exceeding 300 kips.

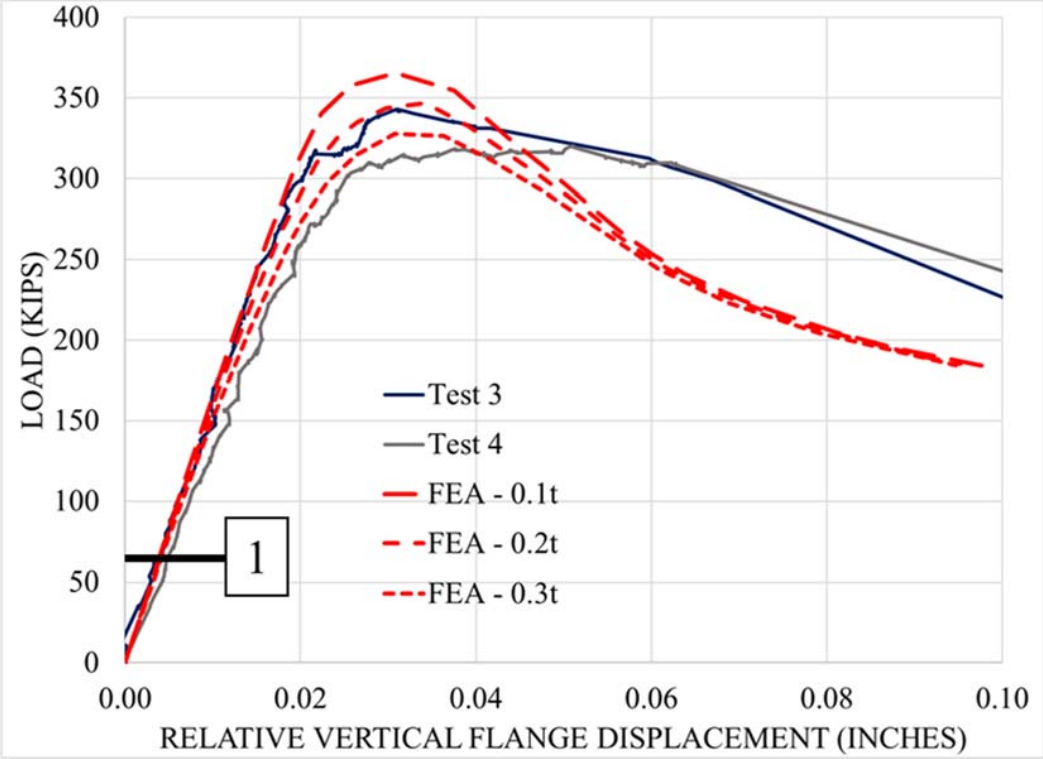

Figure 5: Result Plots of Vertical Flange Displacement

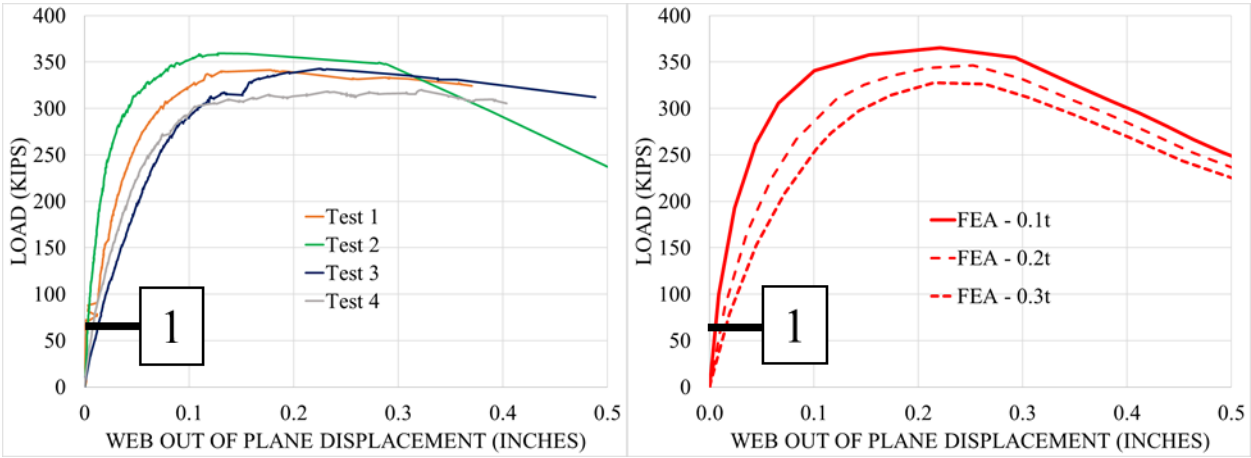

Figure 6: Result Plots of Web Out of Plane Displacement

Numerical results corresponding to initial imperfection parameters of 0.1, 0.2, and 0.3 times the web thickness (t_w) are provided in red dashed lines in the load-displacement response figures. The experimental responses follow the numerically obtained responses closely, and their variance is likely caused by the variations in initial imperfections in the specimens as opposed to a uniformly distributed imperfection associated with a single value prescribed in the numerical model.

Figure 5 shows the vertical flange displacement response of the sustained load tests. The comparisons indicate that the web vertical deformation response recorded in the experimental tests are reasonably represented in the numerical model. Load vs. vertical relative flange displacement (web deformation) responses from only Tests 3 and 4 were reported in the figure, because those tests utilized the modified instrumentation layout with bottom flange DTs. Tests 1 and 2 were conducted before those changes were implemented.

Figure 6 displays the out of plane displacements at the midpoint of the web. The experimental results closely follow the numerical curves associated with imperfection levels of 0.1- and 0.2-times web thickness (t_w), in terms of both stiffness and maximum load. This imperfection range consistently provided accurate response comparisons between the experimental and numerical data for all four tests.

Figure 7 provides a graphical representation of the strain data at the midpoint of the web as the applied load is increased. The experimental results are shown in various colors of solid lines while the numerical results from the finite element analysis are shown by the dashed red lines with initial imperfection levels of 0.1 and 0.2 times the web thickness (t_w). As mentioned earlier, the ultimate buckling load calculated by the numerical model depends on the initial out of plane imperfections assumed in the web, and the experimental results closely align with the curves generated with imperfections set to $0.1t_w$ and $0.2t_w$. The imperfections applied in the numerical model varied along the length and depth of the web plate, but differences are expected between the assumed imperfection profile and the actual which would inherently cause some degree of variance between the results.

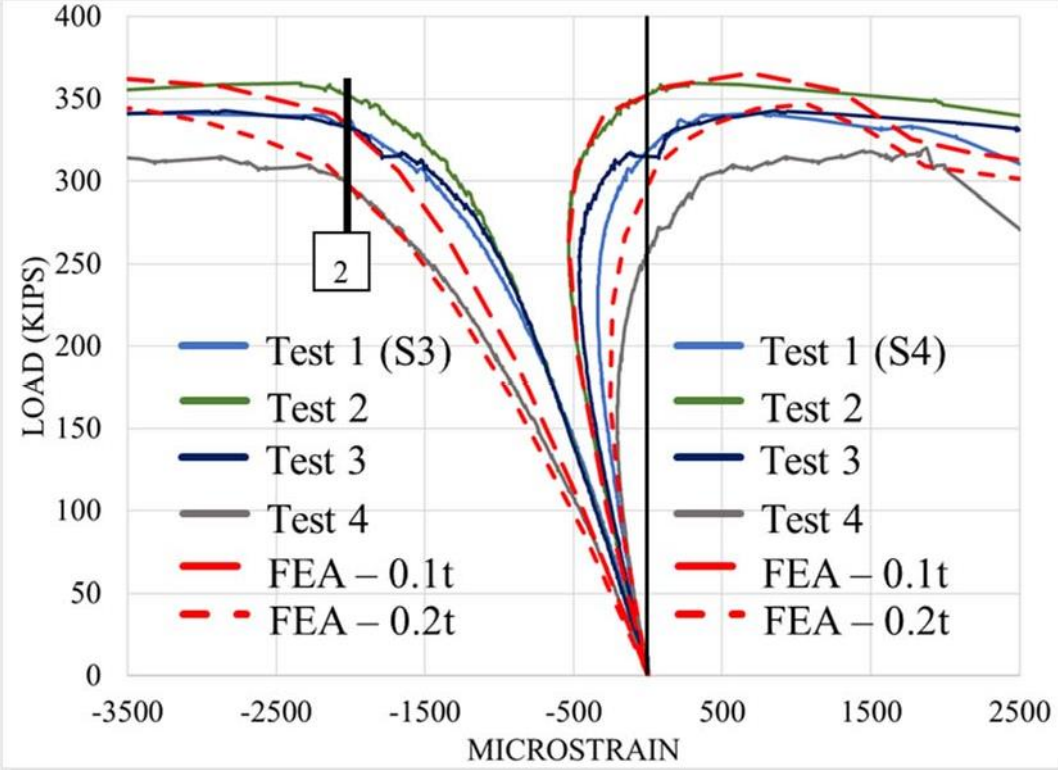

Figure 7: Result Plots of Web Midpoint Strain

Another observation drawn from both the experimental and numerical results relates to the strains at which the specimens reached their peak capacity. The black line noted by point 2 marks the yield strain of the steel specimens, equal to approximately 2000 microstrain. All four specimens had a similar load-strain response trend and experienced buckling shortly after this yield strain was reached and the corresponding strain on the other face of the web reversed to positive (tension) from negative (compression). This pattern is evident in all the experimental tests and can be justified by examining the mechanics of the web plate.

As more load is applied, the web of the specimen deflects in the out of plane direction as shown in Figure 6, resulting in a second order P-δ moment. This P-δ moment must be resisted by a bending moment in the web plate of the specimen to maintain equilibrium.

The moment and curvature caused by this P-δ effect changes the strain profile in the web as shown in Figure 8. The curvature (φ) induced due to the second-order effects causes the difference in strain between the surfaces of the web to increase as well.

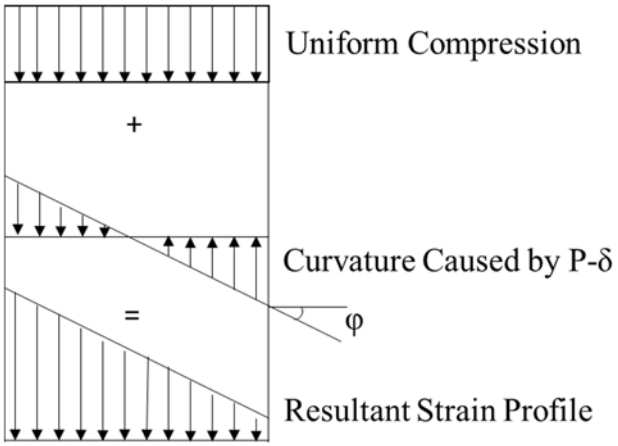

Figure 8: Strain Profile in Web Before Buckling

This increase in curvature will continue as the compressive load increases until the specimen experiences a strain profile similar to the one shown in Figure 9. The strain profile prior to yielding changed proportionally throughout the thickness of the web, allowing the specimen to resist additional load. This was because the steel in the web was still in the elastic range. Once the extreme compression fiber reached yielding, the inability of the yielded fibers to resist additional stresses caused instability and buckling of the web.

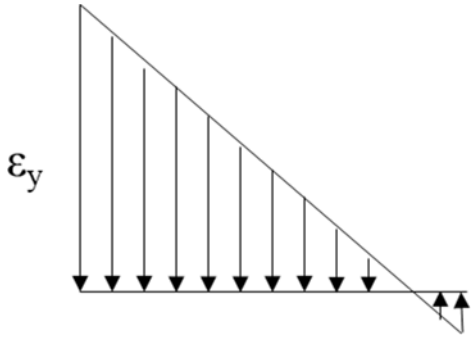

Figure 9: Strain Profile in Web at Buckling

5.2 Influence of Sustained Loading

Figure 10 shows the load and strain responses from the sustained load portions from Tests 3 and 4. The gray and dark blue lines represent the midpoint strains (S3-S4) on either side of the web, while the red and yellow lines represent the applied load variation with time, plotted on a secondary axis. To examine the specimen behavior subjected to sustained loads close to the buckling capacity, the sustained load level was established as the load at which the stress in one face of the web reversed from compressive to tensile, and the other face is experiencing large compressive stress near but slightly less than the yield strain. As mentioned earlier and shown in Figure 7, once tension is experienced on one face of the web, the specimen is very close to its buckling capacity. This load was then sustained for 150 minutes (2.5 hours) and 240 minutes (4 hours) in Tests 3 and 4, respectively.

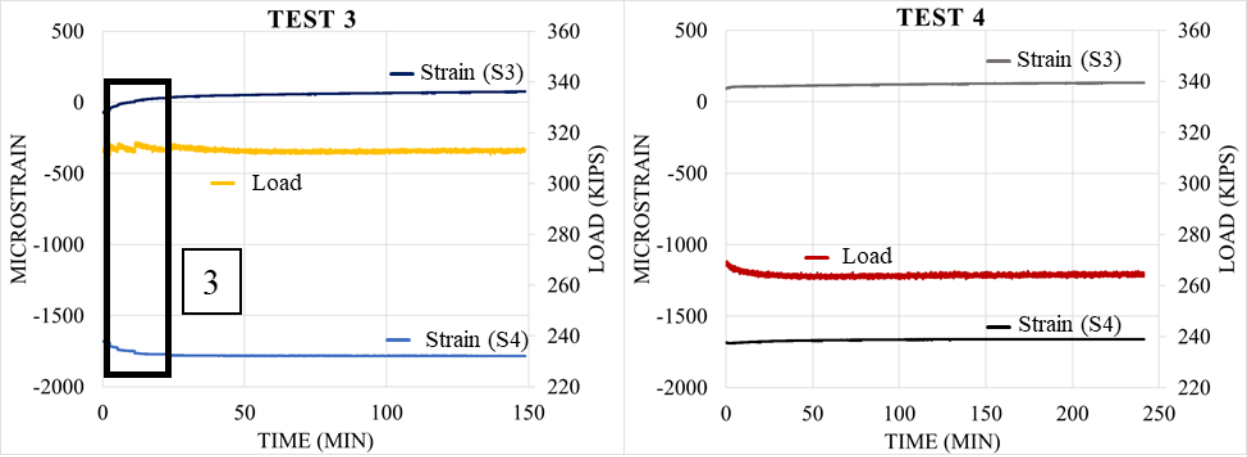

Figure 10: Applied Load and Midpoint Web Strain over Time

The strain-time relationship plots show that there are no significant creep strains induced by the sustained loading irrespective of the duration of loading (2.5 – 4 hours). The loading was applied using a hydraulic actuator, and some hydraulic relaxation occurred initially, which reduced the load slightly (in the range of 1-2%) before reaching a steady-state value. During Test 3, initial attempts were made to account for this relaxation, but this resulted in extending the actuator slightly and applying too much additional loading, which was not desired. This is shown in Figure 10 by the marked-up box and point 3. These initial attempts were terminated, and the applied loading was maintained constant at the steady-state level for the rest of the test duration. Test 4 was conducted without any initial attempts to correct the force due to hydraulic relaxation, which resulted in uniform loading throughout the test after the steady state was reached.

6. Conclusions and Future Work

The loading width has a significant influence on web compression buckling of wide flange steel beams. The current AISC Specification does not include loading width as a parameter for estimating web compression buckling strength. Experimental results indicate that the web compression buckling strength for situations with loading width greater than the beam depth is much higher than that calculated using existing design equations and specification. The compression load capacity of the tested specimens was more than 5 times greater than the web buckling strength calculated using the AISC design equation shown in Eq. 1 (see Table 1 and Figure 5). The modified design equations developed by Menkulasi et al. (2016) were not applicable to the loading condition where the load width was greater than the section depth.

The limit state of web compression buckling also does not have any time-dependent creep effects. Two tests were conducted where the specimens were subjected to a high percentage of loading (83-91% of the web buckling load capacity), which was sustained for a period of 2.5 and 4 hours. In both tests, the strains measured in the webs of the specimens remained steady with time, and there was no evidence of significant creep. The specimens did not creep to buckling failure, and the applied loading had to be increased gradually to cause web compression buckling in the specimens.

3D finite element models were developed and benchmarked using the experimental behavior and results. These models included the effects of geometric imperfections, residual stresses and material inelasticity. These benchmarked models can be used to conduct analytical parametric studies in the near future. The results from experimental and analytical studies can be used to develop design equations that can be used to calculate web compression buckling strength as function of the loading width.

Acknowledgments

This research was conducted at Purdue University's Bowen Laboratory for Large Scale Civil Engineering Research. The steel specimens were donated by Steel Dynamics, Inc. The authors would also like to thank Research Engineer Tom Bradt for his assistance and direction for conducting the experiments.

References

AISC (2016). Specifications for Structural Steel Buildings, ANSI/AISC 360-16, American Institute of Steel Construction, Chicago, IL.

Cheng L, Ping L, Zhenbo Z, Derek N (2001). "Room temperature creep of high strength steel" *Materials and Design*, Elsevier Ltd, 22 (4) 325-328.

Menkulasi, F., Farzana, N., Moen, C.D., Eatherton, M.R. (2016). "Revisiting Web Compressing Buckling for Wide Flange Sections" *Proceedings of the Annual Stability Conference.* Orlando, FL. April 12-15, 2016.